Article

Current Biology

A molecular mechanism for high salt taste in *Drosophila*

Graphical abstract

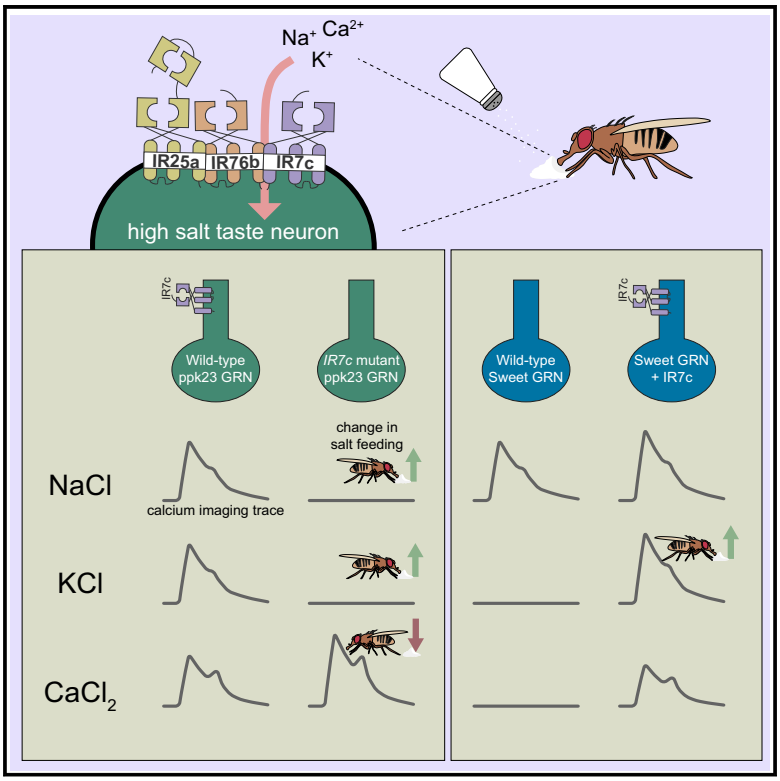

Authors

Sasha A.T. McDowell, Molly Stanley, Michael D. Gordon

Correspondence

gordon@zoology.ubc.ca

In brief

McDowell et al. show that IR7c is a receptor subunit that confers cation non-selective high salt tuning to aversive taste neurons in *Drosophila*. *IR7c* mutants exhibit specific impairment in monovalent salt detection, indicating that different tuning subunits complex with IR25a/IR76b co-receptors to mediate the full breadth of salt taste.

Highlights

- IR7c acts with IR25a and IR76b to form a high salt receptor
- IR7c acts in aversive taste neurons to detect monovalent salts
- IR7c is required for normal avoidance of high monovalent salt concentrations
- IR7c misexpression in sweet taste neurons is sufficient to induce KCl attraction

McDowell et al., 2022, Current Biology *32*, 3070–3081
July 25, 2022
https://doi.org/10.1016/j.cub.2022.06.012

CellPress

CellPress

Current Biology

Article

A molecular mechanism for high salt taste in *Drosophila*

Sasha A.T. McDowell,[1] Molly Stanley,[1] and Michael D. Gordon[1,2,3,*]
[1]Department of Zoology and Life Sciences Institute, The University of British Columbia, Vancouver, BC V6T 1Z3, Canada
[2]Twitter: @Gordonflylab
[3]Lead contact
*Correspondence: gordon@zoology.ubc.ca
https://doi.org/10.1016/j.cub.2022.06.012

SUMMARY

Dietary salt detection and consumption are crucial to maintaining fluid and ionic homeostasis. To optimize salt intake, animals employ salt-dependent activation of multiple taste pathways. Generally, sodium activates attractive taste cells, but attraction is overridden at high salt concentrations by cation non-selective activation of aversive taste cells. In flies, high salt avoidance is driven by both "bitter" taste neurons and a class of glutamatergic "high salt" neurons expressing pickpocket23 (ppk23). Although the cellular basis of salt taste has been described, many of the molecular mechanisms remain elusive. Here, we show that ionotropic receptor 7c (IR7c) is expressed in glutamatergic high salt neurons, where it functions with co-receptors IR76b and IR25a to detect high salt and is essential for monovalent salt taste. Misexpression of IR7c in sweet neurons, which endogenously express IR76b and IR25a, confers responsiveness to non-sodium salts, indicating that IR7c is sufficient to convert a sodium-selective gustatory receptor neuron to a cation non-selective one. Furthermore, the resultant transformation of taste neuron tuning switches potassium chloride from an aversive to an attractive tastant. This research provides insight into the molecular basis of monovalent and divalent salt-taste coding.

INTRODUCTION

Salt is vital for many physiological processes, including electrolyte homeostasis, neuronal transmission, muscle contraction, and nutrient absorption. However, too much salt can produce ill effects. To balance need and excess, both mammals and insects display a concentration-dependent switch in their behavioral response to salt. Generally, sodium becomes increasingly attractive up to ~100 mM and aversive beyond ~250 mM.[1–4]

The appetitive-aversive dichotomy of salt is encoded by the balance of distinct salt-sensitive taste pathways: sodium-specific cells that activate at low concentrations and drive salt consumption, and distinct cation non-selective cells that override attraction at higher concentrations to mediate aversion.[1–8] In mice, a dedicated population of taste receptor cells (TRCs) expressing epithelial sodium channel (ENaC) specifically senses sodium and mediates behavioral attraction to low NaCl.[1] On the other hand, high salt recruits the two main aversive taste pathways—bitter and sour—to promote avoidance.[2] Unlike each of the other primary taste modalities, molecular sensors for high salt remain unclear.

Flies detect tastes using gustatory receptor neurons (GRNs) located in various body parts, including the labellum, legs, and pharynx.[9–11] Salt coding is best understood in the labellum, where 31 taste sensilla are roughly equally divided into short (S-type), long (L-type), and intermediate (I-type) classes.[3,12,13] As in mammals, innately attractive and aversive pathways have been co-opted for salt coding in *Drosophila*. Sweet GRNs, labeled by gustatory receptor 64f (Gr64f), respond selectively to sodium salts and promote consumption.[3,14] A recently defined GRN population expressing IR94e also displays sodium-selective activation and may have a minor impact on attraction.[3] Conversely, higher concentrations of any salt activate two aversive GRN populations that override sodium attraction: bitter GRNs labeled by Gr66a, and a population of pickpocket23 (ppk23)-expressing glutamatergic GRNs ($ppk23^{glut}$).[3,5,15] Although it is a member of the ENaC family, ppk23 is not required for high salt responses in $ppk23^{glut}$ GRNs.[3]

Early insights into the molecular mechanisms of *Drosophila* salt-taste detection revealed that *IR25a* and *IR76b* are necessary for both the sodium-selective salt responses of sweet GRNs and the cation non-selective activity of $ppk23^{glut}$ GRNs.[3,4,16] IR25a and IR76b belong to the ionotropic receptor (IR) family of sensory receptors, which includes 66 members in *Drosophila*, and likely evolved from AMPA or kainate receptors in an ancestral protostome.[17,18] Unlike most IRs, IR25a and IR76b are broadly expressed in chemosensory tissues,[17,19] suggesting roles as co-receptors. Although there are notable exceptions,[20–24] IR-dependent taste, including the taste of salt,[3,14] carbonation,[19] fatty acids,[25] calcium,[15] and acids,[26,27] typically requires both IR25a and IR76b.

Given the evidence for heteromeric assembly of olfactory IR channels from two co-receptors plus a more specific tuning IR subunit, it is likely that each distinct IR25a/IR76b-dependent taste function is mediated by these two co-receptors complexing with an additional IR that confers specific tuning.[19,25,28]

Indeed, a recent study revealed that IR56b is specifically required for appetitive sodium responses in sweet taste neurons and is sufficient to produce sodium sensitivity in heterologous GRNs that express IR25a and IR76b.[14]

Here, we show that IR7c acts with IR25a and IR76b to form a functional high salt receptor. IR7c is expressed in a subset of labellar ppk23^{glut} GRNs that is activated by both monovalent and divalent salts. However, *IR7c* mutants are specifically defective in their physiological responses and behavioral aversion to monovalent salts. Moreover, ectopic expression of IR7c endows sweet neurons with the ability to sense non-sodium salts and overturns the flies' innate KCl aversion in favor of attraction. These findings describe a heteromultimeric IR complex that underlies cation non-selective sensitivity of a key aversive taste cell type and provide insight into the elusive molecular nature of high salt detection.

RESULTS

IR7c functions in high salt taste neurons

We first identified IR7c as a candidate high salt IR based on its reported expression in taste neuron projections resembling those of ppk23^{glut} GRNs.[3,19] Using a *Gal4* knockin to the *IR7c* locus (*IR7c^{Gal4}*) to drive tdTomato expression, we consistently observed one IR7c-expressing GRN in all L-type and a few S-type sensilla in the labellum (Figures 1A and 1B). Co-labeling of *IR7c^{Gal4}* with a *LexA* reporter for ppk23 (*ppk23-LexA*) revealed IR7c expression in all nine L-type ppk23 neurons plus one ppk23-negative GRN in each S4 and S8 sensillum (Figure 1C). Using *VGlut-LexA*, we confirmed the expression of IR7c within L-type glutamatergic neurons; however, the IR7c neuron within S4 and S8 was distinct from the glutamatergic GRN in those sensilla (Figure 1D). We also confirmed the exclusion of IR7c from both bitter (*Gr66a-LexA*) and sweet (*Gr64f-LexA*) GRN populations (Figures 1E and 1F). Thus, IR7c is expressed within the L-type subset of the ppk23^{glut} population, plus a non-glutamatergic GRN in each of the S4 and S8 sensilla (Figure 1H). As expected, IR7c GRN axons projected to the subesophageal zone (SEZ) in a pattern resembling those of ppk23^{glut} (Figure 1G). All the IR7c SEZ projections emanated from the labellar nerve, with no evidence of expression in neurons from the pharynx. However, we noted 1–2 IR7c-expressing GRNs per leg and observed projections to the ventral nerve cord, consistent with those previously reported for ppk23[3,29] (Figure S1).

To determine whether IR7c neurons display functional properties consistent with those of the wider ppk23^{glut} population, we first expressed CsChrimson under the control of *IR7c^{Gal4}* and tested the effect of closed-loop activation in the sip-triggered optogenetic behavior enclosure (STROBE)[30] (Figure 1I). Flies had access to feed on two identical sources of 100 mM sucrose, but interactions with one of the options triggered red LED illumination. Optogenetic activation of IR7c neurons prompted aversion of the light-triggering food, compared with control flies of the same genotype that were not fed the obligate CsChrimson cofactor all-*trans*-retinal (Figure 1I). We next silenced IR7c GRNs using the Kir2.1 potassium channel and measured high salt avoidance using a dye-based binary feeding assay (Figure 1J). Flies were given the option to feed on either 5 mM sucrose or 50 mM sucrose mixed with 500 mM NaCl. This setup incentivizes consumption of the high salt option and expands the behavioral range and sensitivity for detecting differences in avoidance of highly aversive substances.[3,31,32] Control flies avoided the high salt food in favor of the lower sucrose concentration, but flies with silenced IR7c GRNs showed significant impairment in their high salt aversion. Thus, IR7c GRNs carry negative valence and are required for normal avoidance of high salt.

Since IR76b and IR25a are both necessary for high salt detection by ppk23^{glut} GRNs,[3] we postulated that IR7c could be a more specific IR subunit that completes a functional high salt receptor. To detect a role for IR7c in high salt taste, we measured high salt avoidance in *IR7c^{Gal4}* mutants. As predicted, *IR7c* mutants exhibited significant reduction in high salt avoidance, which was restored to control levels by the cell-type-specific expression of *IR7c* (Figure 1K).

IR7c mediates avoidance of high NaCl and KCl

To characterize IR7c's role more fully in salt detection and behavior, we expressed GCaMP7f under the control of *IR7c^{Gal4}* and imaged IR7c GRN axon terminals in the SEZ while stimulating the labellum for 5 s with increasing concentrations of NaCl and KCl (Figures 2A and 2B). IR7c GRNs responded dose-dependently to increasing concentrations of both salts, exhibiting the lack of sodium selectivity characteristic of aversive high salt cells (Figures 2C and 2D). Moreover, this response was lost in *IR7c* mutants and rescued by cell-type-specific expression of *IR7c* (Figures 2C and 2D), further confirming that IR7c labels high salt neurons and is essential for their responses to NaCl and KCl.

We next conducted NaCl and KCl binary-choice assays to assess the flies' preference for increasing concentrations of salt versus water. Control flies that had been kept under NaCl-fed conditions prior to the assay, to maximize salt avoidance, chose water and 50 mM NaCl equally. However, increasing salt concentrations elicited dose-dependent avoidance (Figure 2E). *IR7c* mutants kept under the same NaCl-fed conditions displayed a dramatic reduction in salt aversion (Figure 2E). Notably, there was no sucrose present in these assays. This enhances the effects at lower salt concentrations but creates a floor effect at high concentrations where avoidance is saturated by IR-independent high salt-avoidance mechanisms, including activation of bitter GRNs.[3] Nonetheless, the impact of IR7c on avoiding 500 mM NaCl can be seen in Figure 1K.

Consistent with our past results,[3] control flies that had been deprived of salt for 3 days showed significantly less salt aversion than NaCl-fed flies of the same genotype (comparing *w^{1118}* in Figure 2E and 2F; $p < 0.0001$ by two-way ANOVA with Tukey's post hoc test). Nonetheless, salt-deprived *IR7c* mutants exhibited further reduction in avoidance compared with both salt-deprived controls (Figure 2F) and NaCl-fed *IR7c* mutants (comparing *IR7c* mutants in Figures 2E and 2F; $p < 0.0001$). The results of the KCl binary-choice assay mirrored the NaCl behavioral findings, with the exception that there was no significant difference between the behavior of NaCl-fed and salt-deprived *IR7c* mutants (comparing Figures 2G and 2H; $p = 0.3237$).

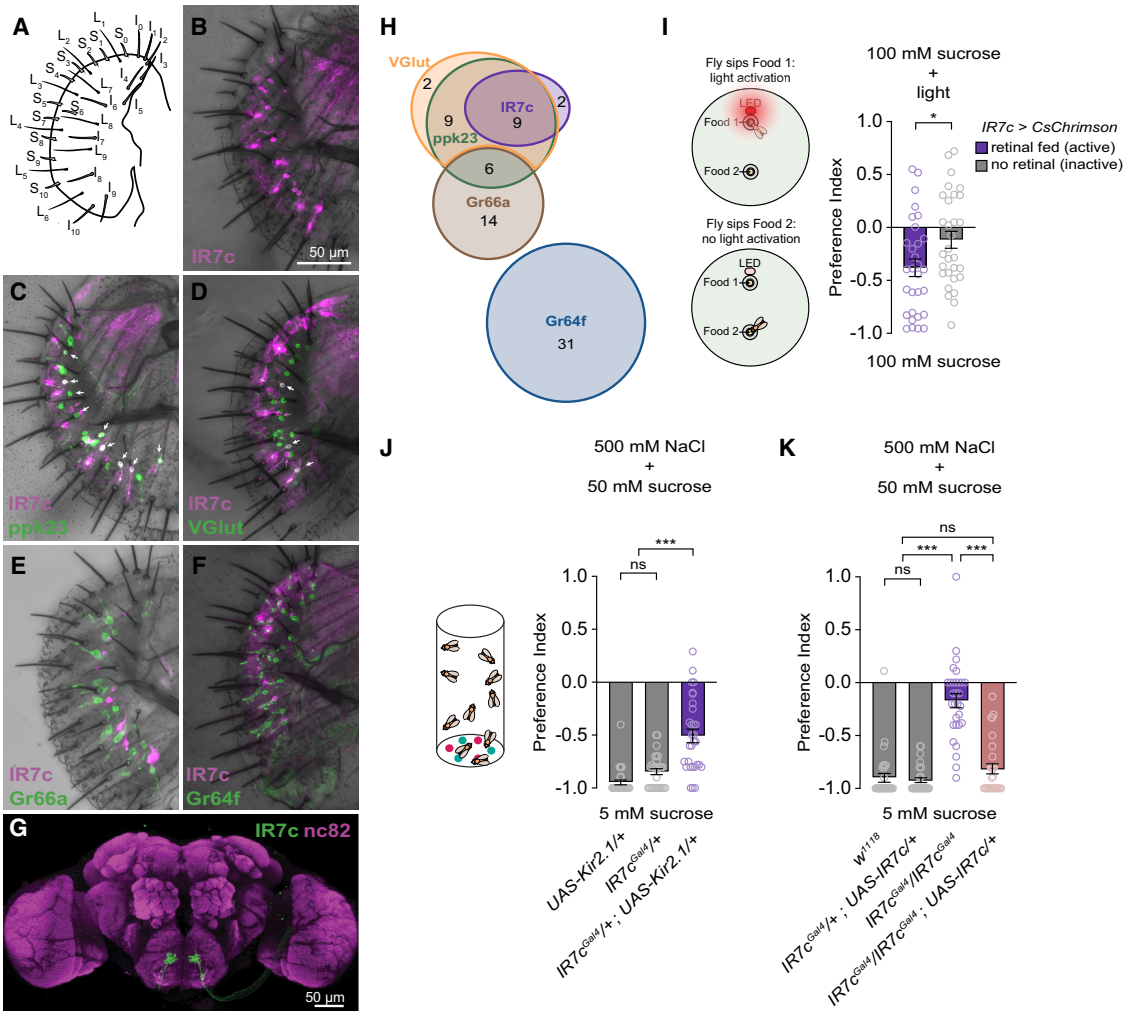

Figure 1. IR7c labels a high salt GRN population

(A) Schematic representation of the fly labellum.

(B–F) Single labellar palps immunolabeled for *IR7c*^{Gal4} driving tdTomato (magenta) alone (B) or in combination with GFP (green) under the control of *ppk23-LexA* (C), *vGlut-LexA* (D), *Gr66a-LexA* (E), or *Gr64f*^{LexA} (F). White arrows indicate overlapping expression, and magenta arrows indicate IR7c-positive cells without overlap.

(G) Immunofluorescence of IR7c GRN projections targeting the SEZ.

(H) Venn diagram illustrating the expression of IR7c in the labellum relative to other GRN markers.

(I) Schematic representation of the closed-loop sip-triggered optogenetic behavior enclosure (STROBE; left) and preference indices for flies expressing CsChrimson in IR7c GRNs and fed retinal (purple) or not-fed retinal (gray). Positive values indicate preference for the light-triggering food. n = 30 flies per condition.

(J) Schematic of binary-choice feeding assay (left) and preference indices for flies expressing Kir2.1 in IR7c GRNs (purple) and controls (gray). Positive values indicate preference for 500 mM NaCl plus 50 mM sucrose; negative values indicate preference for 5 mM sucrose alone. n = 30 groups of ~10 flies each.

(K) Feeding preferences for *IR7c* mutants (purple), controls (gray), and rescue (pink) in the high salt aversion binary-choice assay. n = 30 groups of ~10 flies each.

Bars in all figures represent mean ± SEM with circles indicating individual replicates. Asterisks denote significant difference between groups by unpaired two-tailed t test (I) or one-way ANOVA with Tukey's post hoc test (J and K); *p < 0.05, ***p < 0.001. See also Figure S1.

IR7c is essential for IR-dependent monovalent salt detection

Our next step was to determine the specific tuning of IR7c by conducting calcium imaging with a broader panel of stimuli encompassing different taste modalities (Figure 3A) and different salt species (Figure 3B). IR7c GRNs did not respond to sugar, bitter compounds, acetic acid, or a mixture of amino acids, demonstrating their specificity for salt (Figure 3A). IR7c GRN salt tuning, however, was broad, with strong responses to all salt species tested (Figure 3B). Interestingly, while *IR7c* mutants showed complete loss of responses to all monovalent salts tested (NaCl, KCl, NaBr, and CsCl), there was no effect on the detection of $CaCl_2$ and $MgCl_2$ (Figure 3B). Since the anion species appeared to have no impact, we conclude that IR7c is specifically required for the detection of monovalent cations. This stands in contrast to the broad co-receptors IR25a and IR76b, which are required for detection of both monovalent and divalent salts by IR7c GRNs (Figure 3C).

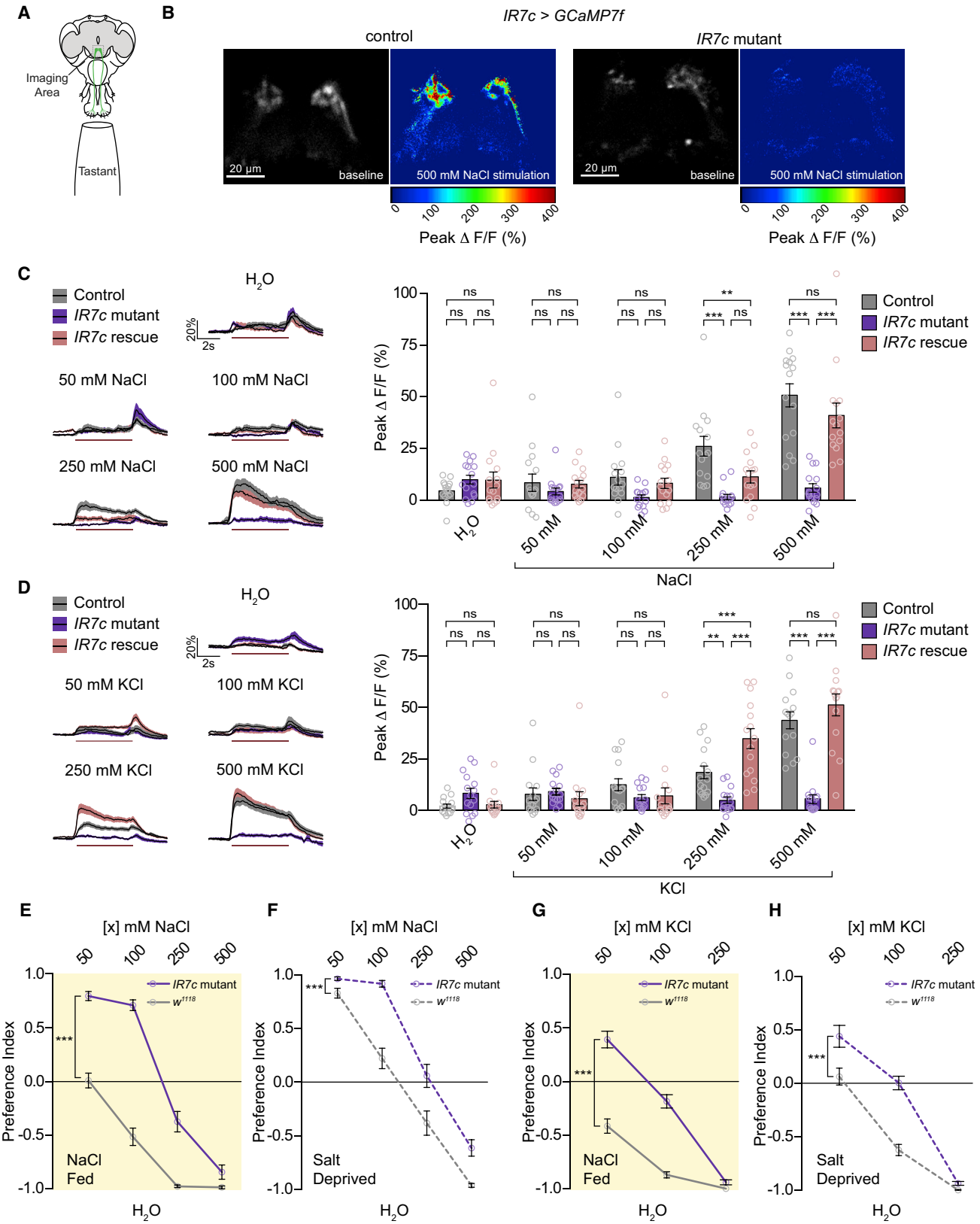

(legend on next page)

Given that IR7c is expressed in only about half of ppk23^{glut} GRNs, we wanted to clarify the extent to which IR7c is responsible for salt-evoked activity across the broader ppk23 population in the labellum. Therefore, we performed calcium imaging of ppk23 neuron salt responses in *IR7c* mutants and isogenic controls (Figure 3D). Ppk23 GRNs displayed the same properties as the IR7c population, with *IR7c* essential for monovalent but not divalent high salt responses (Figure 3D). Therefore, IR7c expression defines the subset of ppk23^{glut} GRNs that encodes monovalent high salt detection.

Next, we extended our imaging studies by examining salt responses in bitter and sweet GRNs. As expected, *IR7c* mutation had no effect on high NaCl responses in sweet (Gr64f) GRNs, which exhibit sodium-specific salt activity[3] (Figure S2A). Bitter GRNs showed little activity to divalent salts, and their monovalent salt responses were largely *IR7c*-independent, although a significant reduction was evident in response to 500 mM KCl (Figure S2B). This result is consistent with our prior observation that bitter GRN salt responses are largely IR25a- and IR76b-independent[3] and with the lack of detectable IR7c expression in bitter neurons. It is unclear whether the small effect observed in *IR7c* mutants is due to weak expression of IR7c that fell below the threshold of detection, or from interactions between bitter and IR7c GRNs. Nonetheless, our calcium imaging of labellar GRNs indicates that IR7c, IR25a, and IR76b are all required components of a monovalent high salt receptor operating primarily in ppk23 GRNs.

IR-dependent salt responses are sensitive to subunit availability

When stimulating IR7c GRNs with 500 mM $CaCl_2$ and $MgCl_2$, we noted a tendency toward higher responses in *IR7c* mutants compared with controls. However, this difference was difficult to tease apart due to a ceiling effect (Figure 3B). Given that calcium is known to be detected at low concentrations,[15] we examined the response of IR7c GRNs to 1 mM concentrations of both divalent salts (Figure 4A). Low concentrations of both salts elicited two peaks of calcium activity, corresponding to stimulus onset and removal. *IR7c* mutants displayed a significantly enhanced onset peak, while the removal peak remained similar (Figure 4A). Consistent with these imaging results, *IR7c* mutants displayed enhanced avoidance of both $CaCl_2$ and $MgCl_2$ at 1 mM (Figure 4B). Notably, although control flies showed no clear behavioral response to 1 mM $MgCl_2$, *IR7c* mutants strongly avoided it. Nonetheless, 10 mM concentrations of both salts are aversive to control and mutant flies (Figure 4B). Thus, loss of IR7c potentiates divalent salt sensitivity in IR7c GRNs.

One potential explanation for potentiated divalent salt responses in *IR7c* mutants is increased availability of IR co-receptors to form a divalent salt receptor with a different tuning IR. Because IR62a has been implicated in sensing low calcium,[15] we explored its involvement in divalent salt detection by IR7c GRNs. Calcium imaging of IR7c GRN divalent salt responses in *IR62a* mutant flies failed to reveal a significant requirement for *IR62a* in detecting $CaCl_2$ or $MgCl_2$ (Figure S3A). There was a trend toward reduced sensitivity to low divalent salt concentrations, including 50 mM $CaCl_2$, which was previously shown to evoke IR62a-dependent electrophysiological responses in labellar taste sensilla, but the effect did not reach significance[15] (Figure S3B). We reasoned that IR62a and IR7c could be partially redundant in their functions. However, flies that were mutant for both *IR7c* and *IR62a* retained normal responses to $CaCl_2$ and $MgCl_2$ (Figure 4C). Thus, we conclude that divalent salt sensitivity in IR7c neurons can be mediated independently of IR7c and IR62a.

As a final test of whether IR62a could contribute to high salt responses in IR7c neurons, we overexpressed IR62a in IR7c GRNs. Interestingly, this caused a drastic reduction in all IR7c GRN salt responses (Figure 4D). Therefore, IR62a appears to antagonize IR7c's function in salt detection, possibly through displacement of IR7c from the IR7c/25a/76b complex. Along with our observation that *IR7c* mutants display elevated calcium and magnesium responses, this suggests that IR-dependent tuning is highly sensitive to subunit dose.

IR7c forms a functional salt receptor with IR25a and IR76b

To establish that IR25a, IR76b, and IR7c complex to form a functional high salt receptor, we aimed to reconstitute this receptor in a heterologous GRN type. We used *Gr64f-Gal4* to express IR7c in sweet neurons, which already express IR25a and IR76b[3,19,24,25,27] (Figure 5A). Strikingly, while sweet neurons normally show responses to only sodium salts, IR7c expression conferred sensitivity to high concentrations of $CaCl_2$ and KCl (Figure 5A). Thus, expression of IR7c was sufficient to convert sweet neurons from a sodium-specific cell type to a cation non-selective one. Interestingly, this experiment also indicated that an IR7c-containing salt receptor is sufficient, but not necessary, for the detection of high divalent salt concentrations. Along

Figure 2. IR7c mediates detection and avoidance of NaCl and KCl

(A) A schematic representation of the calcium imaging preparation.

(B) Heatmaps showing *IR7c>GCaMP7f* GRNs stimulated with 500 mM NaCl in controls (left) and *IR7c* mutants (right).

(C) Calcium imaging of IR7c GRN responses to increasing NaCl concentrations in *IR7c* mutants (purple), isogenic controls (gray) and *IR7c* rescue flies (pink), showing time course (left) and peak fluorescence changes (right). n = 15 flies per group.

(D) IR7c GRN responses to increasing KCl concentrations in *IR7c* mutants and *IR7c* rescue flies. n = 15 flies per group.

(E) Binary-choice feeding preferences of *IR7c* mutants (purple) and isogenic w^{1118} controls (gray) previously fed NaCl. n = 29–30 groups of ~10 flies for each genotype.

(F) Feeding preferences of *IR7c* mutants for NaCl under salt-deprived conditions. n = 30 groups of ~10 flies for each genotype.

(G) Feeding preferences of *IR7c* mutants for KCl under NaCl-fed conditions. n = 30 groups of ~10 flies for each genotype.

(H) Feeding preferences of *IR7c* mutants for KCl under salt-deprived conditions. n = 30 groups of ~10 flies for each genotype.

Calcium imaging trace lines and shaded regions in all figures represent mean ± SEM. Red line beneath traces indicates 5-s stimulation. In binary feeding assays, positive values indicate preference for indicated salt concentration; negative values indicate preference for water. Dots represent mean ± SEM. Asterisks indicate significant difference between groups by two-way ANOVA with Tukey's post hoc test; $^{**}p < 0.01$, $^{***}p < 0.001$.

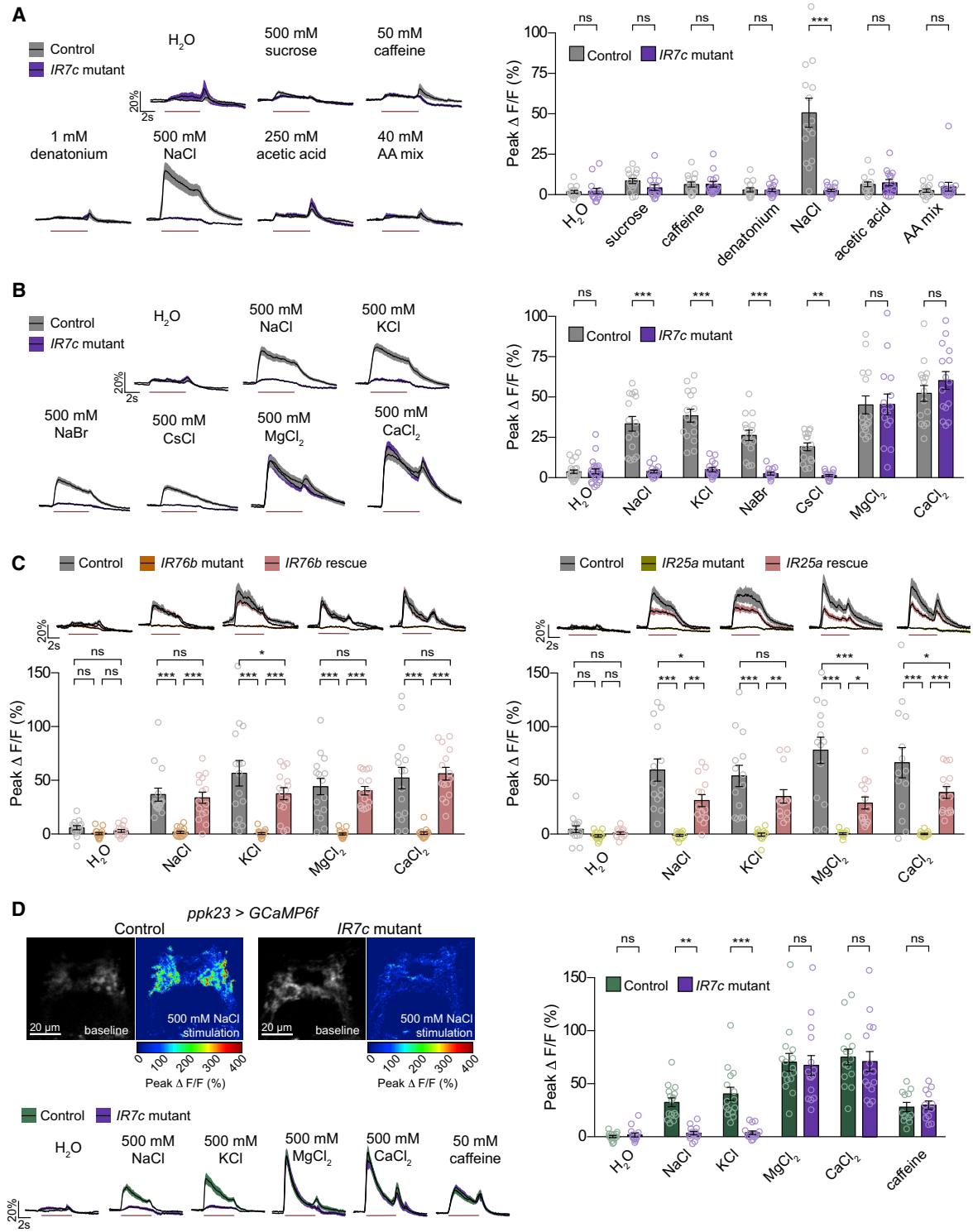

Figure 3. IR7c is essential for monovalent salt detection in ppk23 GRNs

(A) Calcium imaging of IR7c GRN responses to tastants from various modalities in *IR7c* mutants (purple) and controls (gray). n = 15 flies per group.

(B) IR7c GRN responses to various salts in *IR7c* mutants and controls. n = 15–23 flies per group.

(C) IR7c GRN responses to salts in *IR76b* mutants (left; n = 15 flies) and *IR25a* mutants (right; n = 13–14 flies.) Heterozygous controls (gray) and rescue flies (pink) for respective mutants are also shown.

(legend continued on next page)

with the observation that IR7c expression did not endow low $CaCl_2$ sensitivity, this suggests that IR7c/25a/76b form a cation non-specific high salt receptor, but a more sensitive IR25a/76b-dependent divalent salt receptor exists in IR7c GRNs. To further support IR7c's sufficiency in the formation of a high salt receptor, we misexpressed IR7c in a second heterologous GRN population using *IR94e-Gal4*. Wild-type IR94e GRNs display minimal low sodium activation,[3] but we conducted the experiment in an *IR94e* mutant background, which shows no significant high salt-evoked activity (Figure S4A). As with sweet neurons, ectopic expression of *IR7c* in IR94e GRNs produced strong cation non-selective high salt responses (Figure S4A). Notably, reconstituting the IR7c high salt receptor in sweet or IR94e GRNs produced onset and offset peaks to calcium, suggesting that these dynamics are a property of the receptor and not specific to the IR7c GRN type.

Further calcium imaging of sweet GRNs expressing IR7c revealed dose-dependent responses to KCl (Figure 5B). We predicted that transforming the stimulus specificity of these appetitive GRNs would impact flies' feeding on non-sodium salts. KCl, similarly to other non-sodium salts, is generally aversive at all concentrations (Figure 5C). However, flies expressing IR7c in sweet GRNs were attracted to 100 and 200 mM KCl and displayed significantly less aversion to 500 mM KCl (Figure 5C). Therefore, broadening the salt tuning of sweet GRNs is sufficient to induce KCl attraction.

DISCUSSION

This study identifies IR7c as a critical component of the monovalent high salt taste receptor and provides insights into monovalent and divalent salt coding in flies (Figure 6). Moreover, given the recent finding that IR56b complexes with IR25a and IR76b to mediate attractive sodium taste, our discovery of IR7c as a high salt receptor sheds light onto how differences in tuning are achieved in attractive and aversive salt-sensitive taste cells.[3,4,14,16]

Monovalent salt coding

Unlike the peripheral coding of bitter and sweet compounds, which generally follows a labeled-line organization,[5,7,33] monovalent salts are encoded by a combination of most to all GRN classes.[3] Although neural silencing of distinct GRN populations has previously revealed contributions of both bitter and $ppk23^{glut}$ GRNs to high salt avoidance,[3] *IR7c* mutants afford an additional tool to probe the complexity of monovalent salt-taste coding. In particular, the drastic change in behavior toward NaCl seen in *IR7c* mutants highlights the importance of IR7c GRNs in high salt avoidance, although IR7c-independent salt avoidance mechanisms clearly exist (Figure 2E). Interestingly, *IR7c* mutants display attraction toward 50 mM KCl (Figure 2G), despite the lack of detectable KCl-evoked activity in sweet GRNs (Figure 5). The source of this attraction is unclear, but it could be very weak activation of sweet neurons or osmotic effects on ppk28-expressing "water" GRNs.[34,35] Future studies may further dissect IR7c-independent contributions to salt coding through silencing different GRN populations within an *IR7c* mutant background. It will also be interesting to ask whether there are functional differences between the nine glutamatergic L-type IR7c neurons and the two non-glutamatergic IR7c GRNs found in S4 and S8.

We previously suggested that aversion via the $ppk23^{glut}$ salt-specific pathway is suppressed by salt deprivation, thereby fine-tuning salt intake based on need.[3] Consistent with this model, we find that the avoidance of KCl is modulated by salt deprivation in control flies, but not in *IR7c* mutants (Figures 2G and 2H; $p = 0.3237$). Thus, the IR7c salt-taste pathway is necessary for modulation of KCl avoidance by salt need. However, modulation of NaCl avoidance by salt deprivation is only partially suppressed in *IR7c* mutants, as salt-deprived mutants show marginally higher NaCl preference than those that have been previously NaCl fed (Figures 2E and 2F; $p < 0.0001$). Together, these results suggest that sodium-specific attractive salt taste is also modulated (in this case enhanced) by salt deprivation. Finally, it is notable that even among salt-deprived flies, *IR7c* mutants show significantly reduced salt avoidance compared with controls (Figures 2F and 2H). This indicates that our 3-day salt deprivation did not fully suppress the IR7c-dependent pathway to the equivalence of IR7c loss. Whether longer deprivation could more fully suppress this pathway is yet to be tested.

Divalent salt coding

IR7c is not necessary for divalent responses in IR7c GRNs (Figure 3B) or the broader ppk23 population (Figure 3D); however, it is sufficient to confer high $CaCl_2$ responses in sweet neurons (Figure 5A). This suggests that IR7c acts as a cation non-specific high salt receptor, but that at least one more specific divalent salt receptor exists in high salt GRNs. Since consumption of small concentrations of divalent salts can be detrimental to a fly's fitness,[15] receptors that are sensitive to low divalent concentrations are needed to mediate avoidance. This could explain why multiple divalent receptors with different tunings and sensitivities exist within IR7c GRNs.

Based on our findings, IR62a is not responsible for calcium responses in IR7c GRNs. Interestingly, the potentiation of low divalent salt responses observed in IR7c mutants was blunted in *IR62a*, *IR7c* double mutants (Figure 4C), indicating that IR62a may play a role in this effect. However, overall, our IR62a results contrast with a previous report that 50 mM $CaCl_2$ evokes IR62a-dependent electrophysiological activity in select S-type sensilla.[15] S-type ppk23 GRNs do not appear to express IR7c, suggesting that IR62a may mediate calcium detection within IR7c-negative ppk23 neurons. Why flies would have different divalent cation receptors within the IR7c subpopulation of ppk23 GRNs versus outside of it is thought provoking. One clue may exist in the discovery that IR62a antagonizes IR7c GRN salt responses (Figure 4D). How this occurs is unclear, but competition for IR76b and IR25a co-receptors could explain

(D) Heatmaps of *ppk23>GCaMP6f* GRNs stimulated with 500 mM NaCl in isogenic controls (left) and *IR7c* mutants (right). Ppk23 responses in *IR7c* mutants (purple) and controls (green) with time course (bottom left) and peak fluorescence changes (right) for each stimulus. n = 12–15 flies per group.
Asterisks indicate significant difference between groups by two-way ANOVA with Sidak's post hoc test (A, B, and D) or with Tukey's post hoc test (C); *$p < 0.05$, **$p < 0.01$, ***$p < 0.001$. See also Figure S2.

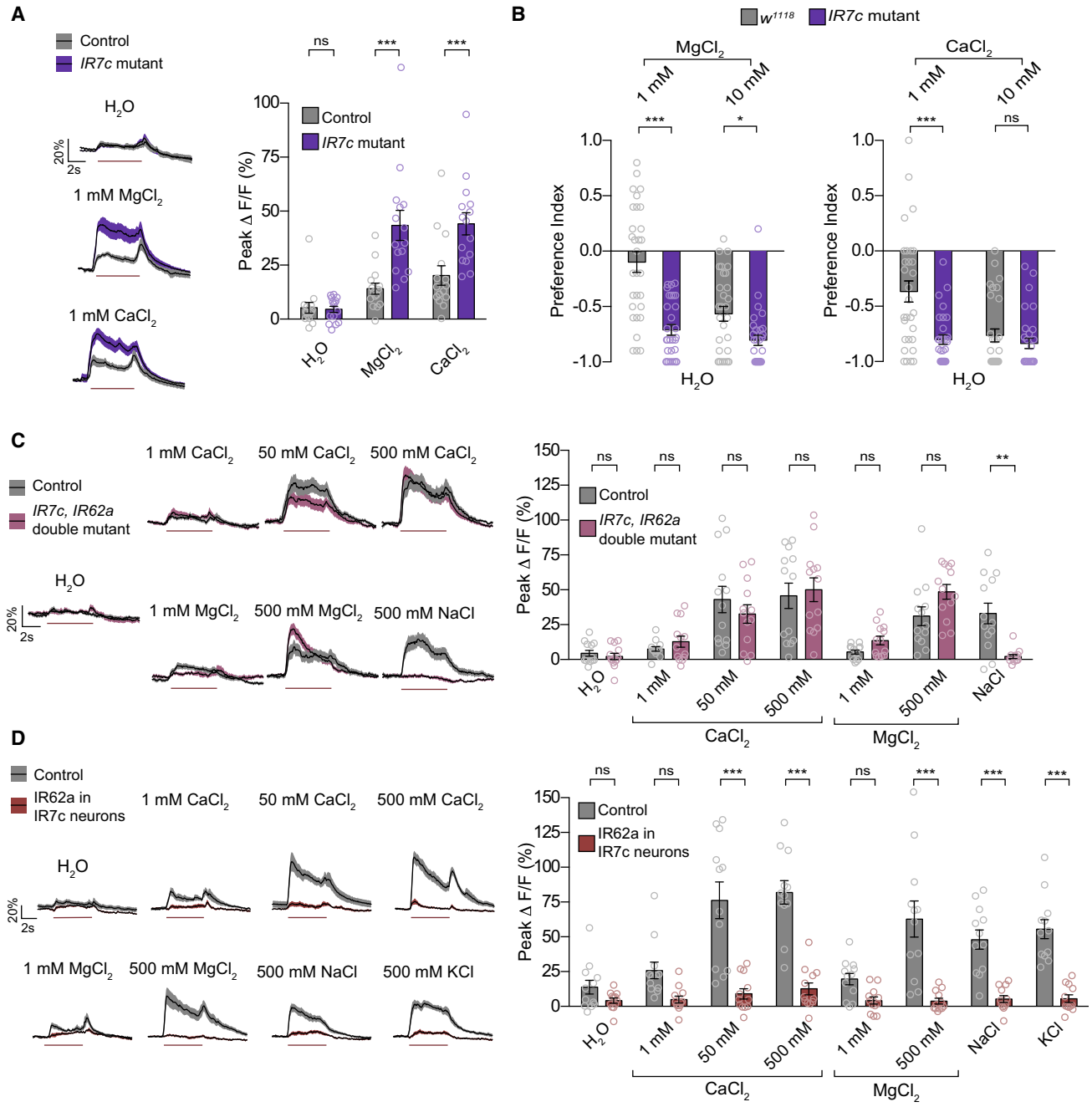

Figure 4. IR7c GRN divalent salt responses do not require IR7c or IR62a

(A) Calcium imaging of IR7c GRN responses to low concentrations of divalent salts in *IR7c* mutants. n = 15 flies per group.

(B) Feeding preferences of *IR7c* mutants for low concentrations of divalent salts in a binary-choice assay. n = 30 groups of ~10 flies for each genotype.

(C) IR7c GRN responses to divalent salts in *IR7c*, *IR62a* double mutants (pink) with isogenic controls (gray). n = 13 flies per group.

(D) IR7c GRN responses to salts in flies expressing IR62a under the control of $IR7c^{Gal4}$ (red) and isogenic controls (gray). n = 12 flies per group.

Asterisks indicate significant difference between groups by two-way ANOVA with Sidak's post hoc test; * $p < 0.05$, ** $p < 0.01$, *** $p < 0.001$. See also Figure S3.

both this phenomenon and the derepression of divalent responses in *IR7c* mutants (Figure 4A). This antagonism is reminiscent of previously reported negative interactions between bitter Grs.[36,37] Alternatively, IRs may compete for space on the membrane, or IR misexpression could affect membrane potential or dynamics, since we noted that IR7c expression in sweet neurons dampened their endogenous Gr-mediated sucrose response (Figure 5). Previous reports of mutual repression between IRs and GRs also fit with this model.[24,38] Regardless, the antagonism between IR62a and IR7c makes it unlikely that these two receptors function within the same neurons unless their expression levels are tightly controlled to ensure appropriate

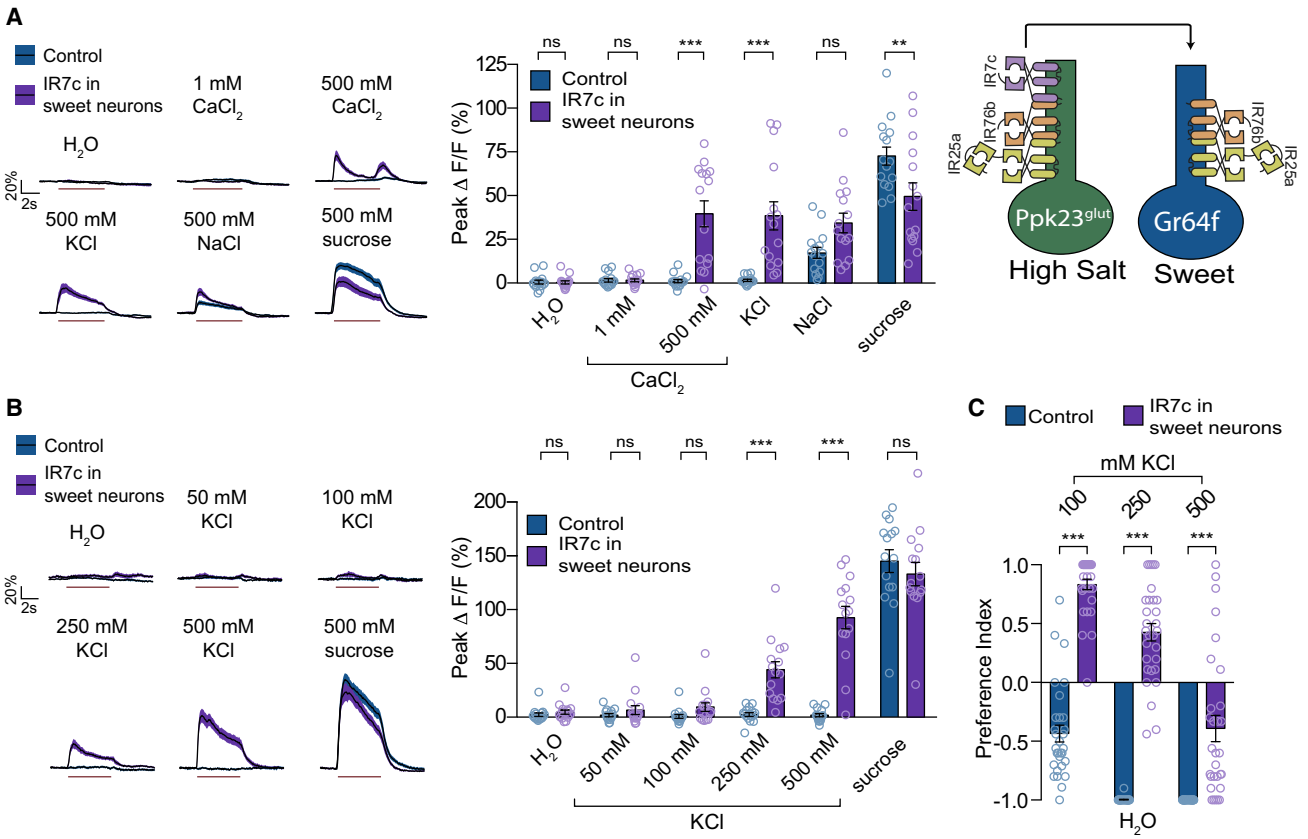

Figure 5. IR7c misexpression broadens salt tuning of sugar-sensing neurons

(A) Calcium imaging of Gr64f GRN salt responses in flies expressing IR7c under the control of *Gr64f-Gal4* (purple) and isogenic controls (blue). n = 15 flies per group.

(B) Gr64f GRN responses to increasing concentrations of KCl in flies with IR7c expression under the control of *Gr64f-Gal4* and isogenic controls. n = 15 flies per group.

(C) Feeding preferences of flies with IR7c expression under the control of *Gr64f-Gal4* and isogenic controls. Positive values indicate preference for indicated KCl concentrations; negative values indicate preference for water. n = 30 groups of ~10 flies each for each genotype.

Asterisks indicate significant difference between groups by two-way ANOVA with Sidak's post hoc test; **p < 0.01, ***p < 0.001. See also Figure S4.

stoichiometry among different receptors. Moreover, perhaps having a divalent receptor outside the IR7c subpopulation of ppk23 GRNs could allow for discrimination between different salt species.

One physiological curiosity relating to divalent salt taste is the two calcium activity peaks corresponding to onset and removal. Similar kinetics have been observed in bitter-GRN responses to bitter substances[39,40] and in sweet-GRN responses to acidic substances.[24] As in bitter taste,[39,40] we find that the same receptor, in our case IR7c, can mediate both onset and removal peaks. It will be interesting to examine the contribution of these temporal dynamics to taste coding. For example, the timing of dopamine-neuron activation derived from bitter off responses influences the direction of plasticity during associative learning.[39] One could imagine a similar role for calcium as an unconditioned stimulus, especially given its reported toxicity.[15] We also note that IR7c neurons display a removal response toward lower osmolarity solutions in both *IR7c* mutants and controls (Figures 2C and 2D). Whether this contributes to IR7c-independent salt behavior is yet unclear.

Modular components of salt taste receptors

In addition to demonstrating necessity of IR7c, IR76b, and IR25a in monovalent high salt detection, we showed that misexpressing IR7c in two different neuronal populations already expressing the co-receptors leads to reconstitution of a high salt receptor (Figure 5). It is formally possible that, by chance, other IR subunits necessary for this high salt receptor are expressed in both IR94e and Gr64f GRNs. However, we consider this possibility improbable. Instead, we postulate that IR25a, IR76b, and IR7c constitute a minimum set of IRs to form a cation non-selective high salt taste receptor. Notably, the lack of sodium responses in IR7c GRNs that are mutant for *IR7c* but still express IR25a and IR76b infers the existence of a key tuning IR subunit for sodium-specific responses in sweet GRNs. Indeed, IR56b was recently found to act with IR25a and IR76b to mediate appetitive responses to sodium.[14] Thus, IR7c and IR56b represent the key to shifting salt detection between sodium-selective and cation non-selective tunings. Interestingly, although sweet GRNs respond in a dose-dependent manner to NaCl, they appear to have a lower threshold for NaCl detection than IR7c

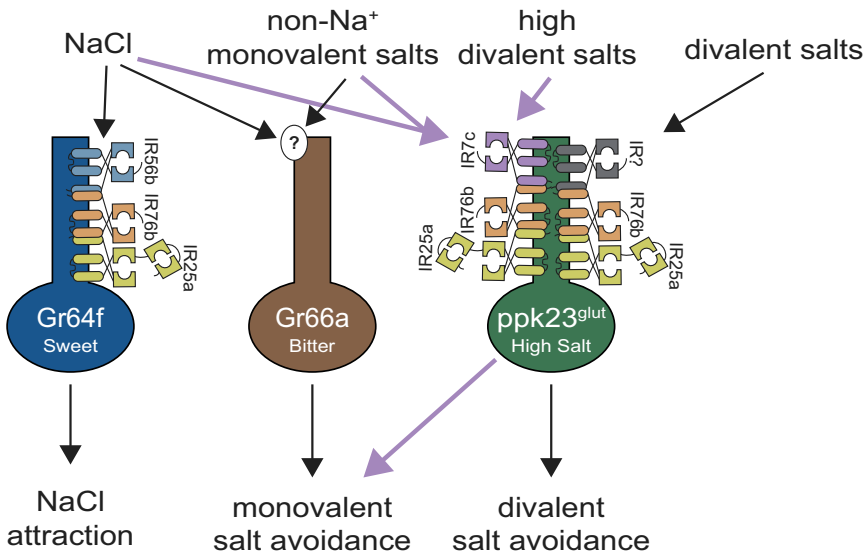

Figure 6. Model for the molecular mechanisms of salt sensing across the main salt-sensitive-GRN populations

Arrows indicate excitation that leads to subsequent behavioral consequences, with roles for IR7c highlighted by purple arrows.

GRNs.[3] Understanding the biophysical mechanisms by which IR56b and IR7c subunits confer changes in both ion selectivity and sensitivity to a salt-taste receptor will be illuminating.

To date, a high salt taste sensor has not been unequivocally identified in mammals. Combining sour-TRC silencing with a *Trpm5* mutation that knocks out the primary effector of the canonical bitter T2R family[41–43] causes complete loss of ENaC-independent NaCl responses in the chorda tympani of mice.[2] Therefore, high salt sensing in bitter TRCs is likely mediated by one or more of the approximate 30 T2Rs.[2] There is also evidence that carbonic anhydrase 4, an enzyme involved in buffering the pH around TRCs, may function to translate external salt into local pH changes, in turn activating the intrinsic sour-TRC mechanism.[2] Although IRs are not conserved in mammals,[18] uncovering their general principles as salt sensors may provide insight into mammalian high salt detection mechanisms.

STAR★METHODS

Detailed methods are provided in the online version of this paper and include the following:

- KEY RESOURCES TABLE
- RESOURCE AVAILABILITY
  - Lead contact
  - Materials availability
  - Data and code availability
- EXPERIMENTAL MODEL AND SUBJECT DETAILS
  - Flies
  - Fly genotypes by figure
  - Generation of transgenic lines
- METHOD DETAILS
  - Tastants
  - Immunohistochemistry
  - Behavioral assays
  - Calcium imaging
- QUANTIFICATION AND STATISTICAL ANALYSIS

SUPPLEMENTAL INFORMATION

Supplemental information can be found online at https://doi.org/10.1016/j.cub.2022.06.012.

ACKNOWLEDGMENTS

We thank Kiereth Atariwala for assistance with binary-choice feeding assays and members of the Gordon lab for comments on the manuscript. We also thank the Bloomington Stock Centre for fly stocks. This work was funded by the Canadian Institutes of Health Research (CIHR) operating grant FDN-148424. M.D.G. is a Michael Smith Foundation for Health Research Scholar.

AUTHOR CONTRIBUTIONS

S.A.T.M. and M.D.G. conceived the project and wrote the manuscript. S.A.T.M performed all experiments. M.S. performed pilot GCaMP imaging and gave experimental advice. M.D.G. supervised the project.

DECLARATION OF INTERESTS

The authors declare no competing interests.

INCLUSION AND DIVERSITY

One or more of the authors of this paper self-identifies as an underrepresented ethnic minority in science. One or more of the authors of this paper self-identifies as a member of the LGBTQ+ community. While citing references scientifically relevant for this work, we also actively worked to promote gender balance in our reference list.

Received: February 25, 2022
Revised: May 4, 2022
Accepted: June 7, 2022
Published: June 29, 2022

REFERENCES

1. Chandrashekar, J., Kuhn, C., Oka, Y., Yarmolinsky, D.A., Hummler, E., Ryba, N.J.P., and Zuker, C.S. (2010). The cells and peripheral representation of sodium taste in mice. Nature *464*, 297–301.
2. Oka, Y., Butnaru, M., von Buchholtz, L., Ryba, N.J.P., and Zuker, C.S. (2013). High salt recruits aversive taste pathways. Nature *494*, 472–475.

3. Jaeger, A.H., Stanley, M., Weiss, Z.F., Musso, P.-Y., Chan, R.C., Zhang, H., Feldman-Kiss, D., and Gordon, M.D. (2018). A complex peripheral code for salt taste in *Drosophila*. eLife *7*, e37167.

4. Zhang, Y.V., Ni, J., and Montell, C. (2013). The molecular basis for attractive salt-taste coding in *Drosophila*. Science *340*, 1334–1338.

5. Marella, S., Fischler, W., Kong, P., Asgarian, S., Rueckert, E., and Scott, K. (2006). Imaging taste responses in the fly brain reveals a functional map of taste category and behavior. Neuron *49*, 285–295.

6. Ishimoto, H., and Tanimura, T. (2004). Molecular neurophysiology of taste in *Drosophila*. Cell. Mol. Life Sci. *61*, 10–18.

7. Wang, Z., Singhvi, A., Kong, P., and Scott, K. (2004). Taste representations in the *Drosophila* brain. Cell *117*, 981–991.

8. Puri, S., and Lee, Y. (2021). Salt sensation and regulation. Metabolites *11*, 175.

9. Stocker, R.F. (1994). The organization of the chemosensory system in *Drosophila melanogaster*: a review. Cell Tissue Res. *275*, 3–26.

10. Singh, R.N. (1997). Neurobiology of the gustatory systems of *Drosophila* and some terrestrial insects. Microsc. Res. Tech. *39*, 547–563.

11. Scott, K. (2018). Gustatory processing in *Drosophila melanogaster*. Annu. Rev. Entomol. *63*, 15–30.

12. Falk, R., Bleiser-Avivi, N., and Atidia, J. (1976). Labellar taste organs of *Drosophila melanogaster*. J. Morphol. *150*, 327–341.

13. Freeman, E.G., and Dahanukar, A. (2015). Molecular neurobiology of *Drosophila* taste. Curr. Opin. Neurobiol. *34*, 140–148.

14. Dweck, H.K.M., Talross, G.J.S., Luo, Y., Ebrahim, S.A.M., and Carlson, J.R. (2022). Ir56b is an atypical ionotropic receptor that underlies appetitive salt response in *Drosophila*. Curr. Biol. *32*, 1776–1787.e4.

15. Lee, Y., Poudel, S., Kim, Y., Thakur, D., and Montell, C. (2018). Calcium taste avoidance in *Drosophila*. Neuron *97*, 67–74.e4.

16. Lee, M.J., Sung, H.Y., Jo, H., Kim, H.-W., Choi, M.S., Kwon, J.Y., and Kang, K. (2017). Ionotropic receptor 76b is required for gustatory aversion to excessive Na+ in *Drosophila*. Mol. Cells *40*, 787–795.

17. Benton, R., Vannice, K.S., Gomez-Diaz, C., and Vosshall, L.B. (2009). Variant ionotropic glutamate receptors as chemosensory receptors in *Drosophila*. Cell *136*, 149–162.

18. Croset, V., Rytz, R., Cummins, S.F., Budd, A., Brawand, D., Kaessmann, H., Gibson, T.J., and Benton, R. (2010). Ancient protostome origin of chemosensory ionotropic glutamate receptors and the evolution of insect taste and olfaction. PLoS Genet. *6*, e1001064.

19. Sánchez-Alcañiz, J.A., Silbering, A.F., Croset, V., Zappia, G., Sivasubramaniam, A.K., Abuin, L., Sahai, S.Y., Münch, D., Steck, K., Auer, T.O., et al. (2018). An expression atlas of variant ionotropic glutamate receptors identifies a molecular basis of carbonation sensing. Nat. Commun. *9*, 4252.

20. Croset, V., Schleyer, M., Arguello, J.R., Gerber, B., and Benton, R. (2016). A molecular and neuronal basis for amino acid sensing in the *Drosophila* larva. Sci. Rep. *6*, 34871.

21. Ganguly, A., Pang, L., Duong, V.-K., Lee, A., Schoniger, H., Varady, E., and Dahanukar, A. (2017). A molecular and cellular context-dependent role for Ir76b in detection of amino acid taste. Cell Rep. *18*, 737–750.

22. Rimal, S., Sang, J., Poudel, S., Thakur, D., Montell, C., and Lee, Y. (2019). Mechanism of acetic acid gustatory repulsion in *Drosophila*. Cell Rep. *26*, 1432–1442.e4.

23. Devineni, A.V., Sun, B., Zhukovskaya, A., and Axel, R. (2019). Acetic acid activates distinct taste pathways in *Drosophila* to elicit opposing, state-dependent feeding responses. eLife *8*, e47677.

24. Stanley, M., Ghosh, B., Weiss, Z.F., Christiaanse, J., and Gordon, M.D. (2021). Mechanisms of lactic acid gustatory attraction in *Drosophila*. Curr. Biol. *31*, 3525–3537.e6.

25. Ahn, J.-E., Chen, Y., and Amrein, H. (2017). Molecular basis of fatty acid taste in *Drosophila*. eLife *6*, e30115.

26. Chen, Y., and Amrein, H. (2017). Ionotropic receptors mediate *Drosophila* oviposition preference through sour gustatory receptor neurons. Curr. Biol. *27*, 2741–2750.e4.

27. Shrestha, B., and Lee, Y. (2021). Mechanisms of carboxylic acid attraction in *Drosophila melanogaster*. Mol. Cells *44*, 900–910.

28. Abuin, L., Bargeton, B., Ulbrich, M.H., Isacoff, E.Y., Kellenberger, S., and Benton, R. (2011). Functional architecture of olfactory ionotropic glutamate receptors. Neuron *69*, 44–60.

29. Thistle, R., Cameron, P., Ghorayshi, A., Dennison, L., and Scott, K. (2012). Contact chemoreceptors mediate male-male repulsion and male-female attraction during *Drosophila* courtship. Cell *149*, 1140–1151.

30. Musso, P.-Y., Junca, P., Jelen, M., Feldman-Kiss, D., Zhang, H., Chan, R.C., and Gordon, M.D. (2019). Closed-loop optogenetic activation of peripheral or central neurons modulates feeding in freely moving *Drosophila*. eLife *8*, e45636.

31. Weiss, L.A., Dahanukar, A., Kwon, J.Y., Banerjee, D., and Carlson, J.R. (2011). The molecular and cellular basis of bitter taste in *Drosophila*. Neuron *69*, 258–272.

32. Chen, Y.-C.D., Park, S.J., Joseph, R.M., Ja, W.W., and Dahanukar, A.A. (2019). Combinatorial pharyngeal taste coding for feeding avoidance in adult *Drosophila*. Cell Rep. *29*, 961–973.e4.

33. Thorne, N., Chromey, C., Bray, S., and Amrein, H. (2004). Taste perception and coding in *Drosophila*. Curr. Biol. *14*, 1065–1079.

34. Chen, Z., Wang, Q., and Wang, Z. (2010). The amiloride-sensitive epithelial Na+ channel PPK28 is essential for *Drosophila* gustatory water reception. J. Neurosci. *30*, 6247–6252.

35. Cameron, P., Hiroi, M., Ngai, J., and Scott, K. (2010). The molecular basis for water taste in *Drosophila*. Nature *465*, 91–95.

36. Delventhal, R., and Carlson, J.R. (2016). Bitter taste receptors confer diverse functions to neurons. eLife *5*, e11181.

37. Dweck, H.K.M., and Carlson, J.R. (2020). Molecular logic and evolution of bitter taste in *Drosophila*. Curr. Biol. *30*, 17–30.e3.

38. Chen, H.-L., Stern, U., and Yang, C.-H. (2019). Molecular control limiting sensitivity of sweet taste neurons in *Drosophila*. Proc. Natl. Acad. Sci. USA *116*, 20158–20168.

39. Devineni, A.V., Deere, J.U., Sun, B., and Axel, R. (2021). Individual bitter-sensing neurons in *Drosophila* exhibit both ON and OFF responses that influence synaptic plasticity. Curr. Biol. *31*, 5533–5546.e7.

40. Snell, N.J., Fisher, J.D., Hartmann, G.G., Talay, M., and Barnea, G. (2020). Distributed representation of taste quality by second-order gustatory neurons in *Drosophila*. Preprint at bioRxiv. https://doi.org/10.1101/2020.11.10.377382.

41. Zhang, Y., Hoon, M.A., Chandrashekar, J., Mueller, K.L., Cook, B., Wu, D., Zuker, C.S., and Ryba, N.J.P. (2003). Coding of sweet, bitter, and umami tastes: different receptor cells sharing similar signaling pathways. Cell *112*, 293–301.

42. Matsunami, H., Montmayeur, J.-P., and Buck, L.B. (2000). A family of candidate taste receptors in human and mouse. Nature *404*, 601–604.

43. Adler, E., Hoon, M.A., Mueller, K.L., Chandrashekar, J., Ryba, N.J.P., and Zuker, C.S. (2000). A novel family of mammalian taste receptors. Cell *100*, 693–702.

44. Baines, R.A., Uhler, J.P., Thompson, A., Sweeney, S.T., and Bate, M. (2001). Altered electrical properties in *Drosophila* neurons developing without synaptic transmission. J. Neurosci. *21*, 1523–1531.

45. Diao, F., Ironfield, H., Luan, H., Diao, F., Shropshire, W.C., Ewer, J., Marr, E., Potter, C.J., Landgraf, M., and White, B.H. (2015). Plug-and-play genetic access to *Drosophila* cell types using exchangeable exon cassettes. Cell Rep. *10*, 1410–1421.

46. Toda, H., Zhao, X., and Dickson, B.J. (2012). The *Drosophila* female aphrodisiac pheromone activates ppk23^{+} sensory neurons to elicit male courtship behavior. Cell Rep. *1*, 599–607.

47. Lai, S.-L., and Lee, T. (2006). Genetic mosaic with dual binary transcriptional systems in *Drosophila*. Nat. Neurosci. *9*, 703–709.

48. Miyamoto, T., Slone, J., Song, X., and Amrein, H. (2012). A fructose receptor functions as a nutrient sensor in the *Drosophila* brain. Cell *151*, 1113–1125.

49. Dahanukar, A., Lei, Y.-T., Kwon, J.Y., and Carlson, J.R. (2007). Two Gr genes underlie sugar reception in *Drosophila*. Neuron *56*, 503–516.

50. Tirian, L., and Dickson, B.J. (2017). The VT GAL4, LexA, and split-GAL4 driver line collections for targeted expression in the *Drosophila* nervous system. Preprint at bioRxiv. https://doi.org/10.1101/198648.

51. Schneider, C.A., Rasband, W.S., and Eliceiri, K.W. (2012). NIH Image to ImageJ: 25 years of image analysis. Nat. Methods *9*, 671–675.

52. Kondo, S., and Ueda, R. (2013). Highly improved gene targeting by germline-specific Cas9 expression in *Drosophila*. Genetics *195*, 715–721.

STAR★METHODS

KEY RESOURCES TABLE

REAGENT or RESOURCE	SOURCE	IDENTIFIER
Antibodies		
Rabbit anti-GFP	Invitrogen	#A11122; RRID: AB_221569
Chicken anti-GFP	Abcam, Cambridge, UK	#13970; RRID: AB_300798
Rabbit anti-RFP	Rockland Immunochemicals, Pottstown, PA	#600-401-379; RRID: AB_2209751
Mouse anti-brp	DSHB	#nc82; RRID: AB_2392664
Goat anti-rabbit Alexa 488	Invitrogen	#A11008; RRID: AB_143165
Goat anti-chicken Alexa 488	Abcam	#150169; RRID: AB_2636803
goat anti-rabbit Alexa 647	Thermo Fisher Scientific	#A21245; RRID: AB_2535813
Goat anti-mouse Alexa 546	Invitrogen	#A11030; RRID: AB_144695
Chemicals, peptides, and recombinant proteins		
All trans-Retinal	Sigma-Aldrich	#R2500
Sucrose	Sigma-Aldrich	#S7903
NaCl	Sigma-Aldrich	#S7653
KCl	Sigma-Aldrich	#P9541
NaBr	Sigma-Aldrich	#S4547
CsCl	Sigma-Aldrich	#289329
$CaCl_2$	BDH chemicals	#BDH4524
$MgCl_2$	BDH chemicals	#BDH0244
Caffeine	Sigma-Aldrich	#C0750
Denatonium benzoate	Sigma-Aldrich	#D5765
Acetic Acid	Sigma-Aldrich	#64-19-7
Serine	Sigma-Aldrich	#84959
Alanine	Sigma-Aldrich	#05129
Phenylalanine	Sigma-Aldrich	#P5482
Glycine	Sigma-Aldrich	#50046
Agar	Sigma-Aldrich	#A1296
Eriglaucine	Spectrum	#FD110
Amaranth	Sigma-Aldrich	#A1016
4% Paraformaldehyde in PBS	Alfa Aesar	#J61899
Deposited data		
Raw data from all Figures	Mendeley Data	https://doi.org/10.17632/y6hjyvksj4.1
Experimental models: Organisms/strains		
D. melanogaster: w^{1118}	Bloomington Drosophila Stock Centre	BDSC: 3605; RRID: BDSC_3605
D. melanogaster: D. melanogaster: IR7c^{Gal4}	This study	N/A
D. melanogaster: UAS-IR7c	This study	N/A
D. melanogaster: UAS-Kir2.1	Baines et al.[44]	Flybase: FBti0017552
D. melanogaster: vGlut^{MI04979}-LexA::QFAD	Diao et al.[45]	BDSC: 60314; RRID: BDSC_60314
D. melanogaster: ppk23-LexA	Toda et al.[46]	Flybase: FBst0051311
D. melanogaster: 20XUAS-CD8::GFP	Bloomington Drosophila Stock Center	B BDSC: 32194; RRID: BDSC_32194
D. melanogaster: 26xLexAop2-mCD8::GFP	Bloomington Drosophila Stock Center	BDSC: 32207; RRID: BDSC_32207
D. melanogaster: LexAop-rCD2::GFP	Lai and Lee[47]	Flybase: FBti0186090
D. melanogaster: UAS-tdTomato	Bloomington Drosophila Stock Center	BDSC: 36327; RRID: BDSC_36327
D. melanogaster: UAS-CD8::tdTomato	Thistle et al.[29]	N/A
D. melanogaster: UAS-CsChrimson	Bloomington Drosophila Stock Center	BDSC: 55135; RRID: BDSC_55135
D. melanogaster: LexAOp-GCaMP6f	Bloomington Drosophila Stock Center	BDSC: 44277; RRID: BDSC_44277

(*Continued on next page*)

Continued

REAGENT or RESOURCE	SOURCE	IDENTIFIER
D. melanogaster: Gr66a-lexA	Thistle et al.[29]	Flybase: FBal0277069
D. melanogaster: Gr64f^{LexA}	Miyamoto et al.[48]	Flybase: FBti0168176
D. melanogaster: UAS-GCaMP7f	Bloomington Drosophila Stock Center	BDSC: 79031; RRID: BDSC_79031
D. melanogaster: UAS-GCaMP7f	Bloomington Drosophila Stock Center	BDSC: 80906; RRID: BDSC_80906
D. melanogaster: IR25a^{1}	Benton et al.[17]	Flybase: FBst0041736
D. melanogaster: IR25a^{2}	Benton et al.[17]	Flybase: FBst0041737
D. melanogaster: UAS-IR25a	Bloomington Drosophila Stock Center	BDSC: 78067; RRID: BDSC_78067
D. melanogaster: IR76b^{1}	Zhang et al.[4]	Flybase: FBst0051309
D. melanogaster: IR76b^{2}	Zhang et al.[4]	Flybase: FBst0051310
D. melanogaster: UAS-IR76b	Zhang et al.[4]	Flybase: FBtp0085485
D. melanogaster: Gr64f-Gal4	Dahanukar et al.[49]	Flyase: FBtp0057275
D. melanogaster: UAS-GCaMP6f	Bloomington Drosophila Stock Center	BDSC: 52869; RRID: BDSC_52869
D. melanogaster: UAS-IR62a	Bloomington Drosophila Stock Center	BDSC: 78069; RRID: BDSC_78069
D. melanogaster: ΔIR62a	Bloomington Drosophila Stock Center	BDSC: 32713; RRID: BDSC_32713
D. melanogaster: UAS-20xGCaMP6f	Bloomington Drosophila Stock Center	BDSC: 42747; RRID: BDSC_42747
D. melanogaster: IR94e-Gal4	Jaeger et al.[3] and Tirian and Dickson[50]	VDRC: v207582
D. melanogaster: IR94e^{LexA}	This study	N/A
Software and algorithms		
STROBE	Musso et al.[30]	N/A
ImageJ	Schneider et al.[51]	https://imagej.nih.gov/ij; RRID: SCR_003
Prism 6	Graphpad	RRID:SCR_002798
Illustrator	Adobe	RRID:SCR_010279

RESOURCE AVAILABILITY

Lead contact

Further information and requests for resources and reagents should be directed to and will be fulfilled by the lead contact, Michael Gordon (gordon@zoology.ubc.ca).

Materials availability

All reagents generated in this study are available from the lead contact without restriction.

Data and code availability

- Raw data has been deposited at Mendeley and is publicly available as of the date of publication. DOI is listed in the key resources table.
- This paper does not report original code.
- Any additional information required to reanalyze the data reported in this paper is available from the lead contact upon request.

EXPERIMENTAL MODEL AND SUBJECT DETAILS

Flies

Drosophila melanogaster of indicated genotypes were raised on a standard cornmeal diet at 25°C in 70% humidity. All experimental flies were 2-10 days mated females unless otherwise stated. Information on flies generated in this study and the genotypes used in each experiment are listed below. Additional source and strain information can be found in the key resources table.

Fly genotypes by figure

Figure 1

- *IR7c^{Gal4}/IR7c^{Gal4}; ppk23-LexA/UAS-CD8::tdTomato; LexAop2-mCD8:GFP/+*
- *IR7c^{Gal4}/+; vGlut-LexA/UAS-CD8::tdTomato; LexAop2-mCD8:GFP/+*
- *IR7c^{Gal4}/Gr66a-LexA; UAS-tdTomato/+; LexAop-rCD2:GFP/+*

- *IR7c*^{Gal4}/+; *LexAop-rCD2:GFP/UAS-CD8::tdTomato*; *Gr64f*^{LexA}/+
- *IR7c*^{Gal4}/*IR7c*^{Gal4}; +/+; *UAS-CD8::GFP*/+
- *IR7c*^{Gal4}/*IR7c*^{Gal4}; *UAS-CsChrimson*/+; +/+
- +/+; +/+; *UAS-Kir2.1*/+
- *IR7c*^{Gal4}/+; +/+; +/+
- *IR7c*^{Gal4}/+; +/+; *UAS-Kir2.1*/+
- *w*^{1118}
- *IR7c*^{Gal4}/+; +/+; *UAS-IR7c*/+
- *IR7c*^{Gal4}/*IR7c*^{Gal4}; +/+; +/+
- *IR7c*^{Gal4}/*IR7c*^{Gal4}; +/+; *UAS-IR7c*/+

Figure 2

- *IR7c*^{Gal4}/+; +/+; *UAS-GCaMP7f/UAS-GCaMP7f*
- *IR7c*^{Gal4}/*IR7c*^{Gal4}; +/+; *UAS-GCaMP7f*/+
- *IR7c*^{Gal4}/*IR7c*^{Gal4}; +/+; *UAS-GCaMP7f/UAS-IR7c*
- *IR7c*^{Gal4}/*IR7c*^{Gal4}; +/+; +/+
- *w*^{1118}

Figure 3

- *IR7c*^{Gal4}/+; +/+; *UAS-GCaMP7f/UAS-GCaMP7f*
- *IR7c*^{Gal4}/*IR7c*^{Gal4}; +/+; *UAS-GCaMP7f*/+
- *IR7c*^{Gal4}/+; *UAS-GCaMP7f*/+; *IR76b*^{1}/+
- *IR7c*^{Gal4}/+; *UAS-GCaMP7f*/+; *IR76b*^{1}/*IR76b*^{2}
- *IR7c*^{Gal4}/+; *UAS-GCaMP7f/UAS-IR76b*; *IR76b*^{1}/*IR76b*^{2}
- *IR7c*^{Gal4}/+; *IR25a*^{1}/+; *UAS-GCaMP7f*/+
- *IR7c*^{Gal4}/+; *IR25a*^{1}/*IR25a*^{2}; *UAS-GCaMP7f*/+
- *IR7c*^{Gal4}/+; *IR25a*^{1}/*IR25a* ^{2}, *UAS-IR25a*; *UAS-GCaMP7f*/+
- *IR7c*^{Gal4}/*IR7c*^{Gal4}; *ppk23-LexA/ LexAOp-GCaMP6f*; +/+
- *IR7c*^{Gal4}/+; *ppk23-LexA/ LexAOp-GCaMP6f*; +/+

Figure 4

- *IR7c*^{Gal4}/+; +/+; *UAS-GCaMP7f/UAS-GCaMP7f*
- *IR7c*^{Gal4}/*IR7c*^{Gal4}; +/+; *UAS-GCaMP7f*/+
- *IR7c*^{Gal4}/*IR7c*^{Gal4}; +/+; +/+
- *w*^{1118}
- *IR7c*^{Gal4}/+; *UAS-GCaMP7f/UAS-GCaMP7f*; *ΔIR62a*/+
- *IR7c*^{Gal4}/*IR7c*^{Gal4}; *UAS-GCaMP7f*/+; *ΔIR62a/ΔIR62a*
- *IR7c*^{Gal4}/+; +/+; *UAS-GCaMP7f*/+
- *IR7c*^{Gal4}/+; +/*UAS-IR62a*; *UAS-GCaMP7f*/+

Figure 5

- +/+; *Gr64f-Gal4*, *UAS-GCaMP6f*/+; +/+
- +/+; *Gr64f-Gal4*, *UAS-GCaMP6f*/+; *UAS-IR7c*/+
- +/+; *Gr64f-Gal4*/+; +/+
- +/+; *Gr64f-Gal4*/+; *UAS-IR7c*/+

Figure S1:

- *IR7c*^{Gal4}/*IR7c*^{Gal4}; +/+; *20XUAS-CD8::GFP*/+
- *IR7c*^{Gal4}/*IR7c*^{Gal4}; +/+; *20XUAS-CD8::GFP/20XUAS-CD8::GFP*

Figure S2:

- *IR7c*^{Gal4}/*IR7c*^{Gal4}; *Gr66a-lexA/ LexAOp-GCaMP6f*; +/+
- *IR7c*^{Gal4}/+; *Gr66a-lexA/ LexAOp-GCaMP6f*; +/+
- *IR7c*^{Gal4}/*IR7c*^{Gal4}; +/*LexAOp-GCaMP6f*; *Gr64f*^{LexA}/+
- *IR7c*^{Gal4}/+; +/*LexAOp-GCaMP6f*; *Gr64f*^{LexA}/+

Figure S3:

- *IR7c*^{Gal4}/+; *UAS-GCaMP7f/UAS-GCaMP7f*; *ΔIR62a/+*
- *IR7c*^{Gal4}/+; *UAS-GCaMP7f/UAS-GCaMP7f*; *ΔIR62a/ΔIR62a*

Figure S4:

- +/+; *UAS-20xGCaMP6f/+*; *IR94e-Gal4*, *IR94e*^{LexA}/*IR94e*^{LexA}
- +/+; *UAS-20xGCaMP6f/+*; *UAS-IR7c*, *IR94e*^{LexA}/*IR94e-Gal4*, *IR94e*^{LexA}

Generation of transgenic lines

The *IR7c*^{Gal4} line was created by deleting most of the coding DNA sequence (CDS) and replacing it with Gal4::VP16 using CRISPR/Cas9-mediated genome editing with homology-dependent repair. Upstream gRNA sequence GCAACATCGTGTTTCATCGG[TGG] and downstream gRNA sequence GATTTGTGGTCAAGATCTCC[AGG] were cloned into the U6 promoter plasmid. Upstream and downstream homology arms of *IR7c* were amplified by PCR and subcloned into the pUC57-Kan vector with a *Gal4::VP16-RFP* cassette containing Gal4::VP16, 3xP3-RFP, and two loxP sites. IR7c-targeting gRNAs and hs-Cas9 were microinjected with the donor plasmid into a *w*^{1118} control strain. F1 flies carrying the selection marker were validated by genomic PCR and sequencing. The resulting deletion was 1919bp, from -12th nucleotide relative to ATG to -65th nt relative to stop codon of *IR7c*. The entire procedure was performed by WellGenetics (Taipei City, Taiwan) using a modified version of previously published methods.[52]

The *IR94e*^{LexA} line was created using a similar method as *IR7c*^{Gal4} with the exception that the IR94e CDS was deleted and replaced by *nls-LexA::P65*. The gRNA sequences were TGCCCAAAGTGGATCCTGAG[CGG] and TTCCAGCAGCCAAACTAGCG[AGG]

The upstream and downstream homology arms of *IR94e* were amplified by PCR and subcloned into pUC57-Kan vector with *nls-LexA::P65-RFP* cassette containing *nls-LexA::P65-RFP*, two loxP sites, and 3xP3-RFP. The resulting deletion was 1843bp, from the start codon "ATG" to -49th nucleotide relative to the *Ir94e* stop codon. The entire procedure was performed by WellGenetics (Taipei City, Taiwan) using a modified version of previously published methods.[52]

The *UAS-IR7c* transgenic line was created by synthesizing the coding sequence of *IR7c* and subcloning into the NotI site of the PUAST-attB vector. Synthesis and cloning were performed by Bio Basic (Ontario, Canada). The transformation vector was injected into *w*^{1118} embryos for PhiC31c-mediated integration into the attP2 site. Injections were performed by Rainbow Transgenic Flies (California, USA).

METHOD DETAILS

Tastants

The following tastants were used: sucrose, NaCl, $MgCl_2$, $CaCl_2$, caffeine, denatonium, acetic acid, serine, alanine, phenylalanine, glycine, NaBr, CsCl. All tastants were kept as 1M stocks and diluted as necessary for experiments.

Immunohistochemistry

Immunofluorescent imaging of labella was carried out as previously described.[3] For single labelling experiments, the primary antibody used was rabbit anti-GFP (1:1000, Invitrogen) and goat anti-rabbit Alexa 488 (1: 200, Invitrogen). For co-labeling experiments, chicken anti-GFP (1:1000, Abcam) and rabbit anti-RFP (1:200, Rockland Immunochemicals) were used as primary antibodies and goat anti-chicken Alexa 488 (1:200, Abcam) and goat anti-rabbit Alexa 647 (1:200, Thermo Fisher Scientific) were used as the secondary antibodies.

Brain immunofluorescence was performed as previously described.[3] Primary antibodies used were rabbit anti-GFP (1:1000, Invitrogen) and mouse anti-brp (1:50, DSHB #nc82). Secondary antibodies used were goat anti-rabbit Alexa 488 and goat anti-mouse Alexa 546 (1:200, Invitrogen).

All images were acquired using a Leica SP5 II Confocal microscope with a 25x water immersion objective. Images were processed in ImageJ.[51] For labellar analysis, confocal z-stacks of 2-8 labella were examined to identify neurons in each sensilla that were positive for the different drivers and where there was overlap.

Behavioral assays

STROBE experiments were performed as previously described.[30] Mated female flies 2-3 days post eclosion were placed into vials containing 1 mL standard cornmeal food supplemented with 1 mM all-trans-retinal (Sigma-Aldrich) or an ethanol vehicle control for 2 days in the dark. Flies were starved for 24 hours on 1% agar supplemented with 1 mM all-trans-retinal, prior to experimentation. Both channels of the STROBE arenas were loaded with 4 μl of 100 mM sucrose. The STROBE software was started and single flies were placed into each arena via mouth aspiration. Experiments ran for 60 minutes, and the preference index for each fly was calculated as: (sips from Food 1 – sips from Food 2)/(sips from Food 1 + sips from Food 2).

Binary choice feeding assays were conducted as previously described.[3] Flies aged 2–5 days were sorted into groups of 10 and placed in NaCl fed conditions (1% agar, 5% sucrose, and 10 mM NaCl). Flies were then 24-hr starved on 1% agar and 10 mM NaCl prior to tests. For salt deprived experiments flies were placed on 1% agar and 5% sucrose for 3 days. They were 24-hr starved on 1% agar prior to tests. For all binary choice preference tests, flies were shifted into testing vials containing six 10 μL drops that alternated in color. Each drop contained the indicated concentration of tastant in 1% agar with either blue (0.125mg/mL Erioglaucine,

FD and C Blue#1) or red (0.5mg/mL Amaranth, FD and C Red#2) dye. Each time a binary choice experiment was run, approximately half the replicates were done with the dye swapped to control for any dye preference. Flies were allowed to feed for 2 hours in the dark at 29°C before being frozen at −20°C. A dissection microscope was used to score the color of the abdomen as red, blue, purple, or no color. Preference Index (PI) was calculated as ((# of flies labeled with tastant 1 color) - (# of flies labeled with tastant 2 color))/ (total # of flies with color) and accounted for any flies that were lost in vial transferal and those that did not eat. Any vials with <7 flies or <30% of flies feeding were excluded.

Calcium imaging

Calcium imaging experiments were performed as previously described.[3] Prior to *in vivo* GCaMP imaging of the GRN axon terminals, flies were briefly anesthetized with CO_2 and placed in a custom chamber. Nail polish was used to secure the back of the neck and a little wax was applied to both sides of the proboscis in an extended position, covering the maxillary palps without touching the labellar sensilla. After 1 hr recovery in a humidity chamber, antennae were removed along with a small window of cuticle to expose the SEZ. Adult hemolymph-like (AHL) solution (108 mM NaCl, 5 mM KCl, 4 mM NaHCO3, 1 mM NaH2PO4, 5 mM HEPES, 15 mM ribose, 2mM Ca^{2+}, 8.2mM Mg^{2+}, pH 7.5) was immediately applied. Air sacs and fat were removed and the esophagus was clipped and removed for clear visualization of the SEZ.

A Leica SP5 II Confocal microscope was used to capture GCaMPf fluorescence with a 25x water immersion objective. The SEZ was imaged at a zoom of 4x or 6x, line speed of 8000 Hz, line accumulation of 2, and resolution of 512 × 512 pixels. Pinhole was opened to 2.86 AU. For each taste stimulation, 20 total seconds were recorded. This consisted of 10 s baseline, 5 s stimulation, 5 s post-stimulation. A pulled capillary filed down to fit over both labellar palps was filled with tastant and positioned close to the labellum with a micromanipulator. For the stimulation, the micromanipulator was manually moved over the labellum and then removed from the labellum after 5 s. Each fly was stimulated only once with a particular tastant, and the stimulator was washed with water in between tastants of differing solutions. Salts were applied in order of increasing concentration and all solutions were applied in random order to control for potential inhibitory effects between modalities.

The maximum change in fluorescence (peak $\Delta F/F_0$) for peaks was calculated using peak intensity (average of 3 time points) minus the average baseline intensity (10 time points), divided by the baseline. ImageJ was used to quantify fluorescence changes and create heatmaps.

QUANTIFICATION AND STATISTICAL ANALYSIS

Statistical analyses were performed with GraphPad Prism 6 software. The number of biological replicates using different flies for each experiment and the statistical test performed is given in the figure legend. Sample sizes were determined ahead of experimentation based on the variance and effect sizes observed in prior experiments of similar types. Experimental conditions and controls were run in parallel. Data from calcium imaging experiments were excluded if there was too much movement during the stimulation to reliably quantify the response or if there was no response to a known, robust, positive control. The data from individual flies was removed from STROBE analyses if the fly did not pass a set of minimum sip threshold (15), or the data showed signs of a technical malfunction.